Modeling and operating point analysis for aquatic translational motion of a cross-medium vehicle

Minghao Dou[12], Xuchen Liu[12], Dongyue Huang[12], Biao Wang[34], Jinqiang Cui[4], Qinyuan Ren[5] Lihua Dou[64], Jie Chen[1], Ben M. Chen[2]

1. Shanghai Research Institute for Intelligent Autonomous Systems, Tongji University, Shanghai, China.
E-mail: chenjie206@tongji.edu.cn.

2. Department of Mechanical and Automation Engineering, The Chinese University of Hong Kong, Shatin, N.T., Hong Kong
E-mail: mhdou@mae.cuhk.edu.hk, xcliu@mae.cuhk.edu.hk, dyhuang@mae.cuhk.edu.hk, bmchen@cuhk.edu.hk.

3. College of Automation Engineering, Nanjing University of Aeronautics and Astronautics, Nanjing, Jiangsu, P.R. China
E-mail: wangbiao@nuaa.edu.cn

4. Peng Cheng Laboratory, Shenzhen, Guangdong, China.
E-mail: cuijq@pcl.ac.cn.

5. College of Control Science and Engineering, Zhejiang University, Hangzhou, Zhejiang, China.
E-mail: latepat@gmail.com.

6. Automation, Beijing Institute of Technology, Beijing, China.
E-mail: doulihua@bit.edu.cn

Abstract: Modeling of cross-medium vehicles with complex shapes still requires a thorough investigation. This paper proposes a multi-method combination modeling approach to tackle such a problem. First-principle model is derived to determinate a model structure. Experiments are then set up to estimate parameters related to its rigid-body model and propulsion system. Computational fluid dynamics (CFD) is performed to calculate and identify coefficients related to surrounding fluid. Base on the model obtained, we systematically investigate the possible steady motion of the cross-medium vehicle and analyze their related performance. Results are instrumental for designing controllers for the vehicle to perform autonoumous missions.

Key Words: Unmanned vehicles, Modeling, Cross-medium, Operationg points, CFD

1 Introduction

Cross-medium vehicles that are able to navigate in aerial and aquatic environments have received great interest in recent years. Based on this idea, multiple designs of aerial-aquatic vehicles have been studied and produced (see for example a recent survey paper by Tan and Chen [1]). According to the propulsion method, these designs are divided into multirotor-based aerial–aquatic vehicles [2–5] and fixed-wing vehicles [6–8]. Methods for establishing accurate dynamics model of underwater vehicles still require more effort. Due to working environments, aerial and aquatic model are established accordingly. Aerial motion of these vehicles is similar to conventional drones, corresponding modeling work is less difficult. For aquatic motion, hydrodynamic effect is amplified and results in the coupling of different channels. Besides, compared with the streamlined autonomous underwater vehicles (AUV), shape of a cross-medium vehicle is more complex, which brings more difficulties to modeling works. In addition, due to the complex aquatic environment and waterproof requirements, traditional identification experimental methods are difficult to directly applied in water. Above problems lead to huge challenge in aquatic modeling works.

Aerial motion modeling of drones has been studied for decades, corresponding methods are proved to be effective [9]. For aquatic modeling problems, reasonable first-principle modeling is critical. Fossen [10] proposed a model structure in six-degree-of-freedom (6 DOF) equations for underwater rigid body. This model structure is widely accepted. Besides the model structure, parameter estimation becomes the key point, especially those related to hydrodynamics. For vehicles in complex shapes, existing methods for calculating these parameters include: experimental identification and numerical simulation methods.

Experimental identification method has been studied for decades. It mainly includes the method relying on the Planar Motion Mechanism (PMM). This designed PMM is able to drive the vehicle in water tank and record data at the same time [11, 12]. The result of this method is reliable. The other method use onboard sensors for identification [13]. This methods is less accurate but have higher reproducibility and much lower cost.

Numerical simulation methods use computational fluid dynamics (CFD) software to simulate the fluid around the vehicle and calculate parameters. This method can be applied on vehicles with complex shapes, such as [14, 15]. These researches demonstrate the feasibility of this method. In this paper, we establish the model of TJ-FlyingFish of [8] for theoretical analysis. In this process, multiple modeling methods are applied.

The rest of this paper is organized as follows. Section 2 describes the hardware platform. Section 3 models the vehicle by first-principle method. Section 4 states the experimental identification part. Section 5 propose the CFD works. Section 6 states operating point calculation. Conclusions are given in Section 7.

2 Hardware Platform Description

2.1 Hardware Design of TJ-FlyingFish UAAV

The TJ-FlyingFish cross-medium vehicle designed by our team is shown in the Figure 1. The electronic components are located inside the hemispherical cabin [5]. As shown in Figure 1, four specially designed aerial-aquatic propul-

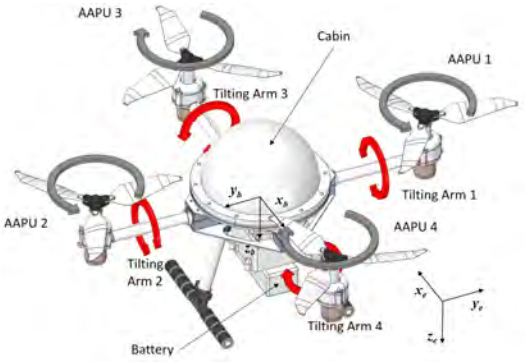

Fig. 1: The structure of TJ-FlyingFish UAAV.

(a) heave(down) (b) heave(up)

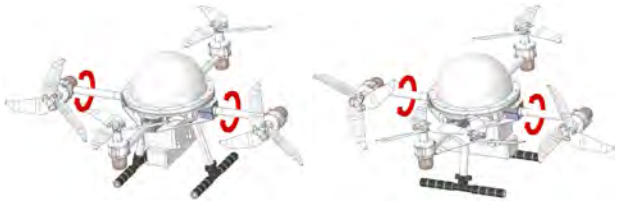

(c) surge (d) sway

Fig. 2: Tilting mechanism of UAAV aquatic motion

sion units (AAPU) are applied to drive the vehicle in both medium. At the connection of arms and cabin, servo motors are applied to implement tilting mechanism. The schematic diagram of propeller rotation and tilting arms are shown in Figure 1. The application of tilting arms improves the maneuverability of aquatic motion. The connection parts of each component have been waterproofed, flange connections are used to seal the connection, which is the basis of underwater functionality.

2.2 Working Mechanism of TJ-FlyingFish

For aerial motion, four AAPUs are all vertically upward, and the layout of the vehicle is consistent with a conventional quadrotor. The layout is exactly the same as shown in Figure 1, no tilting arm is activated. For aquatic motion, 3-axis movement of the vehicle is decomposed into surge, sway and two directions of heave. At present, our heave up and down movement is carried out when pitch and roll angle are approximately zero. For aquatic translational motion, tilting mechanism is activated. This mechanism is shown in Figure 2. For surge and sway motion, tilting is involved to ensure the stability of the vehicle attitude. By combining the aerial and aquatic mechanism, the UAAV is able to complete the 6-DOF motion in both medium.

3 First-Principle Modeling

First-principle model includes kinematics part and dynamics part. These model equations are stated as follows.

3.1 Kinematics Model

Kinematics model mainly includes the transformation between coordinate systems, which is consistent in aerial and aquatic environments. The global and body-fixed coordinates are defined in Figure 1. The origin of body-fixed coordinate locates at the center of gravity (CoG). Equations of kinematics model are shown as follow:

$$\begin{aligned}\dot{x} = {} & u\cos\psi\cos\theta - v(\cos\phi\sin\psi - \cos\psi\sin\phi\sin\theta) \\ & + w(\sin\phi\sin\psi + \cos\phi\cos\psi\sin\theta)\end{aligned} \tag{1}$$

$$\begin{aligned}\dot{y} = {} & u\cos\theta\sin\psi + v(\cos\phi\cos\psi + \sin\phi\sin\psi\sin\theta) \\ & - w(\cos\psi\sin\phi - \cos\phi\sin\psi\sin\theta)\end{aligned} \tag{2}$$

$$\dot{z} = -u\sin\theta + v\cos\theta\sin\phi + w\cos\phi\cos\theta \tag{3}$$

$$\dot{\phi} = p + q\sin\phi\tan\theta + r\cos\phi\tan\theta \tag{4}$$

$$\dot{\theta} = q\cos\phi - r\sin\phi \tag{5}$$

$$\dot{\psi} = \frac{q\sin\phi}{\cos\theta} + \frac{r\cos\phi}{\cos\theta} \tag{6}$$

where x, y, z represent the position of UAAV in global coordinate and ϕ, θ, ψ are Euler angulars for attitude. u, v, w are velocity and p, q, r are angular velocity in body-fixed coordinate.

3.2 Dynamics Model

Due to the great difference in the properties of water and air, in this section, dynamics models of aerial and aquatic motion are proposed separately.

3.2.1 Dynamics Model of Aerial Motion

Rigid-body dynamics of aerial motion is:

$$\dot{u} = \frac{1}{m}(X_P - X_D) + vr - wq - g\sin\theta \tag{7}$$

$$\dot{v} = \frac{1}{m}(Y_P - Y_D) + wp - ur + g\cos\theta\sin\phi \tag{8}$$

$$\dot{w} = \frac{1}{m}(Z_P - Z_D) + uq - pv + g\cos\theta\cos\phi \tag{9}$$

$$\dot{p} = \frac{1}{I_x}[K_P - K_D - (I_z - I_y)qr] \tag{10}$$

$$\dot{q} = \frac{1}{I_y}[M_P - M_D - (I_x - I_z)rp] \tag{11}$$

$$\dot{r} = \frac{1}{I_z}[N_P - N_D + (I_x - I_y)pq] \tag{12}$$

where m is mass and I_x, I_y, I_z are moment of inertia. g is the acceleration of gravity. X_P, Y_P, Z_P, K_P, M_P, N_P are forces and moments generated by propulsion system. X_D, Y_D, Z_D, K_D, M_D, N_D represent damping effect from the medium. For aerial motion, damping forces and moments are:

$$X_D = (X_{u_1} + X_{u|u|_1}|u|)u \tag{13}$$

$$Y_D = (Y_{v_1} + Y_{v|v|_1}|v|)v \tag{14}$$

$$Z_D = (Z_{w_1} + Z_{w|w|_1}|w|)w \tag{15}$$

$$K_D = (K_{p_1} + K_{p|p|_1}|p|)p \tag{16}$$

$$M_D = (M_{q_1} + M_{q|q|_1}|q|)q \tag{17}$$

$$N_D = (N_{r_1} + N_{r|r|_1}|r|)r \tag{18}$$

3.2.2 Dynamics Model of Aquatic Motion

For aquatic motion, added mass and buoyancy effect are included. Based on the aerial dynamics, aquatic dynamics is organized:

$$\dot{u} = \frac{1}{m}(X_P - X_D - X_A - X_{C_A}) + vr - wq - g(1 - \frac{\rho V}{m})\sin\theta \tag{19}$$

$$\dot{v} = \frac{1}{m}(Y_P - Y_D - Y_A - Y_{C_A}) + wp - ur + g(1 - \frac{\rho V}{m})\cos\theta\sin\phi \tag{20}$$

$$\dot{w} = \frac{1}{m}(Z_P - Z_D - Z_A - Z_{C_A}) + uq - pv + g(1 - \frac{\rho V}{m})\cos\theta\cos\phi \tag{21}$$

$$\dot{p} = \frac{1}{I_x}[K_P - K_D - K_A - K_{C_A} - (I_z - I_y)qr + \rho g V z_B \cos\theta\sin\phi] \tag{22}$$

$$\dot{q} = \frac{1}{I_y}[M_P - M_D - M_A - M_{C_A} - (I_x - I_z)rp + \rho g V z_B \sin\theta] \tag{23}$$

$$\dot{r} = \frac{1}{I_z}[N_P - N_D - N_A - N_{C_A} + (I_x - I_y)pq] \tag{24}$$

where ρ is the density of water, V is the volumn of UAAV. X_A, Y_A, Z_A, K_A, M_A, N_A are added mass coefficients in aquatic motion [10]. For aerial motion, added mass effect is ignored. Due to the different properties of air and water, parameters related to damping are different:

$$X_D = (X_{u_2} + X_{u|u|_2}|u|)u \tag{25}$$

$$Y_D = (Y_{v_2} + Y_{v|v|_2}|v|)v \tag{26}$$

$$Z_D = (Z_{w_2} + Z_{w|w|_2}|w|)w \tag{27}$$

$$K_D = (K_{p_2} + K_{p|p|_2}|p|)p \tag{28}$$

$$M_D = (M_{q_2} + M_{q|q|_2}|q|)q \tag{29}$$

$$N_D = (N_{r_2} + N_{r|r|_2}|r|)r \tag{30}$$

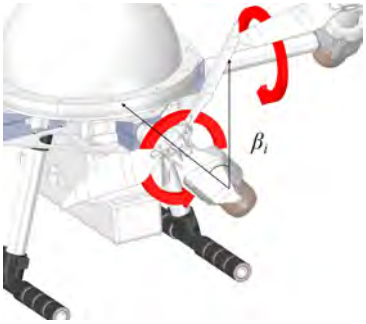

Fig. 3: Tilting angle of arms

3.2.3 Dynamics Model of Propulsion System

For the i-th AAPU, the generated force T and moment Q are marked as T_i and Q_i. As we discussed in section 2.1, for propulsion system in air:

$$X_P = 0, Y_P = 0, Z_P = \sum_{i=1}^{4} T_i \tag{31}$$

$$K_P = (T_1 - T_2)L \tag{32}$$

$$M_P = (T_3 - T_4)L \tag{33}$$

$$N_P = Q_1 + Q_2 - Q_3 - Q_4 \tag{34}$$

Tilting mechanism exists in aquatic motion. As shown in Figure 3, β_i is the tilting angle of i-th arm. We define the positive rotation direction of tilting arms as counterclockwise. For aquatic motion, we have:

$$X_P = T_1\sin\beta_1 - T_2\sin\beta_2 \tag{35}$$

$$Y_P = -T_3\sin\beta_3 + T_4\sin\beta_4 \tag{36}$$

$$Z_P = T_1\cos\beta_1 + T_2\cos\beta_2 + T_3\cos\beta_3 + T_4\cos\beta_4 \tag{37}$$

$$K_P = (T_1\cos\beta_1 - T_2\cos\beta_2)L + Q_1\sin\beta_1 + (-T_3\sin\beta_3 + T_4\sin\beta_4)z_t - Q_2\sin\beta_2 \tag{38}$$

$$M_P = (-T_3\cos\beta_3 + T_4\cos\beta_4)L + Q_3\sin\beta_3 + (-T_1\sin\beta_1 + T_2\sin\beta_2)z_t - Q_4\sin\beta_4 \tag{39}$$

$$N_P = (T_1\sin\beta_1 + T_2\sin\beta_2 + T_3\sin\beta_3 + T_4\sin\beta_4)L + Q_1\cos\beta_1 + Q_2\cos\beta_2 - Q_3\cos\beta_3 - Q_4\cos\beta_4 \tag{40}$$

where z_t is the height difference between the intersection point of four arms and the CoG. L is the arm length. In addition to the above equations that include tilting, dynamics model of single AAPU is also required. In both medium, force and moment generated by a single propulsion unit is approximated as being proportional to the square of the blade speed. For our case, for better matching of experimental results, this model structure is modified. For AAPU in aerial environments:

$$T = K_{t_{11}}^2\omega_m^2 + K_{t_{12}}\omega_m \tag{41}$$

$$Q = K_{q_{11}}^2\omega_m^2 + K_{q_{12}}\omega_m \tag{42}$$

For aquatic environments:

$$T = K_{t_{21}}^2\omega_m^2 + K_{t_{22}}\omega_m \tag{43}$$

$$Q = K_{q_{21}}^2\omega_m^2 + K_{q_{22}}\omega_m \tag{44}$$

where ω_m is the rotation speed of motor.

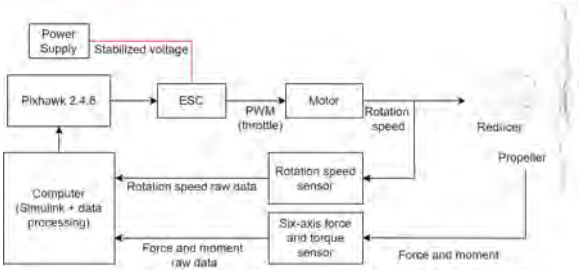

(a) Schematic of experiment set up.

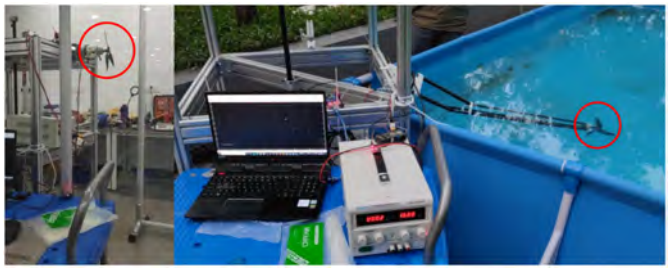

(b) Experiment set up for AAPU aerial (left) and aquatic mode (right) identification.

Fig. 4: AAPU identification experiments.

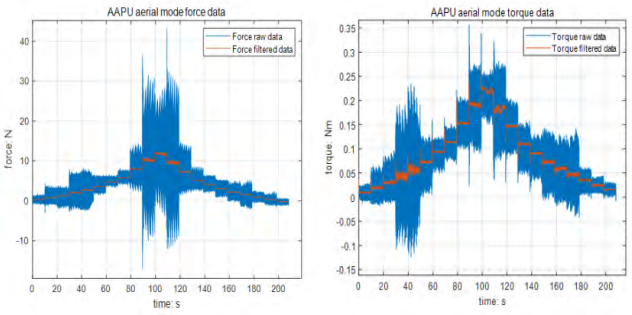

(a) Aerial data

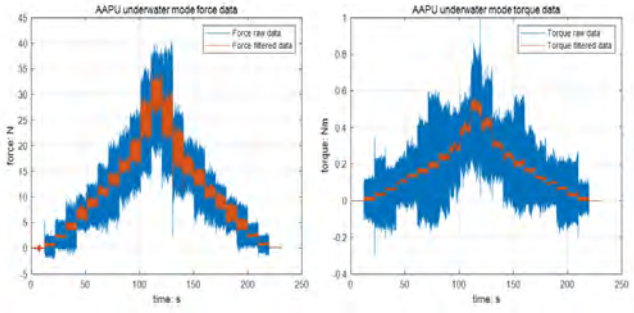

(b) Aquatic data

Fig. 5: AAPU force and torque data.

4 Experimental Identification

Parameters related to the rigid body of the vehicle are directly measured by experiments. These experiments includes measurement of mass, moment of inertia and center of buoyancy. Measurement methods of these parameters are mature, related experiments have reference to previous researches [16] [17].

In order to obtain the parameters in dynamics model of AAPU, identification experiments are designed and performed in aerial and aquatic environments. The diagram of experiment is shown in Figure 4(a), which includes main parts of the experiment. In the experiment, we apply step input PWM signal in AAPU to generate different steady states. The signal is generated by Pixhawk 2.4.8 combining with corresponding toolbox in Simulink. As shown in Figure 4(a), force, torque and motor speed are measured by applied sensors. The experiment set up is applied in both aerial and aquatic environments. The actual experiments are shown in Figure 4(b), AAPU parts are highlighted in the red circle of the figure. Collected force and moment data is shown in Figure 5. As shown in the red lines of the figures, raw data is filtered for calculation. Using these data, parameters in equations (41) to (44) are identified. The complete AAPU dynamics model for steady states is established.

Identified aerial AAPU model is:

$$T = 1.1587 \times 10^{-7}\omega_m^2 + 2.8619 \times 10^{-5}\omega_m \quad (45)$$

$$Q = 1.6430 \times 10^{-9}\omega_m^2 + 2.5078 \times 10^{-6}\omega_m \quad (46)$$

For aquatic motion:

$$T = 2.5604 \times 10^{-7}\omega_m^2 + 0.0006\omega_m \quad (47)$$

$$Q = 5.1233 \times 10^{-9}\omega_m^2 + 1.81713 \times 10^{-7}\omega_m \quad (48)$$

5 Calculation of Hydrodynamic Parameters

5.1 CFD setup

Since the following analysis only includes the operating point calculation, which does not involve accelerated motion. In this section, we only present calculation of damping coefficients. To simplify this modeling problem, tilting angles and blade rotation are not considered in this part. Differences between surge and sway layouts are also ignored.

The CFD software ANSYS Fluent is applied for parameter calculation. Since damping effect exists in all 6-DoF movements, the corresponding simulation in ANSYS Fluent is proposed. Surge, sway and heave are included for translation motion simulations. Pitch, roll and yaw are included for attitude motion simulation. To exclude the effect of added mass, simulation in this part is set in constant velocities. The simulation setup in Fluent is shown as Figure 6. The motion of UAAV is simulated by setting fluid flow movement. The next step is meshing, established grids are shown in Figure 7.

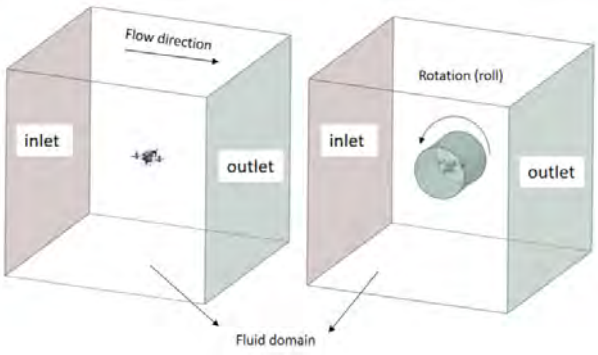

Fig. 6: Setup of computational domains.

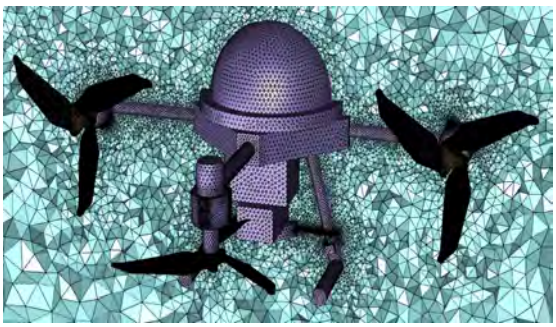

(a) Surge

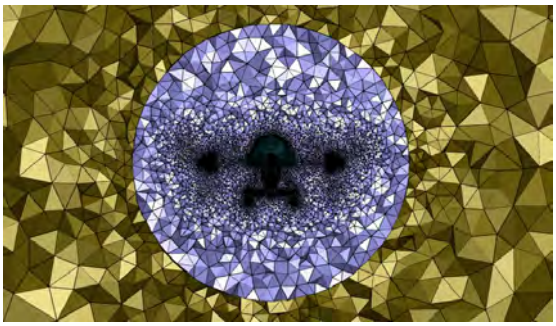

(b) Roll

Fig. 7: Volumn meshing of TJ-FlyingFish.

5.2 Calculation results

A series of solution settings are settled after meshing parts. Due to medium differences, two groups of calculation are performed basing on water and air. A series of translational and rotational velocities are defined for 6-DoF motion. External forces and moments on the vehicle are recorded in the simulation to calculate hydrodynamic parameters. Simulation results are shown in Figure 8. Parameters in equation (25) to (30) are calculated. For aerial motion, ignoring small magnitude parts, we have:

$$\begin{aligned} X_{u_1} &= 0.0010 \quad & X_{u|u|_1} &= 0.0165 \\ Y_{v_1} &= 0.0006 \quad & Y_{v|v|_1} &= 0.0227 \\ Z_{w_1} &= 0.0004 \quad & Z_{w|w|_1} &= 0.0364 \\ K_{p_1} &= 0 \quad & K_{p|p|_1} &= 0.0002 \\ M_{q_1} &= 0 \quad & M_{q|q|_1} &= 0.0005 \\ N_{r_1} &= 0 \quad & N_{r|r|_1} &= 0.0013 \end{aligned} \tag{49}$$

For aquatic motion, we have:

$$\begin{aligned} X_{u_2} &= 0.0998 \quad & X_{u|u|_2} &= 18.2222 \\ Y_{v_2} &= 0.1658 \quad & Y_{v|v|_2} &= 15.8047 \\ Z_{w_2} &= 0.0064 \quad & Z_{w|w|_2} &= 24.7142 \\ K_{p_2} &= 0.0032 \quad & K_{p|p|_2} &= 0.0489 \\ M_{q_2} &= 0.0008 \quad & M_{q|q|_2} &= 0.1554 \\ N_{r_2} &= 0.0029 \quad & N_{r|r|_2} &= 0.1872 \end{aligned} \tag{50}$$

6 Analysis of Operating Points in Aquatic Motion

By combining the contents of previous sections, the dynamics model of aquatic surge and sway mode is established. To explore the possibility of stable motion that the vehicle can perform in water, operating points of the aquatic model

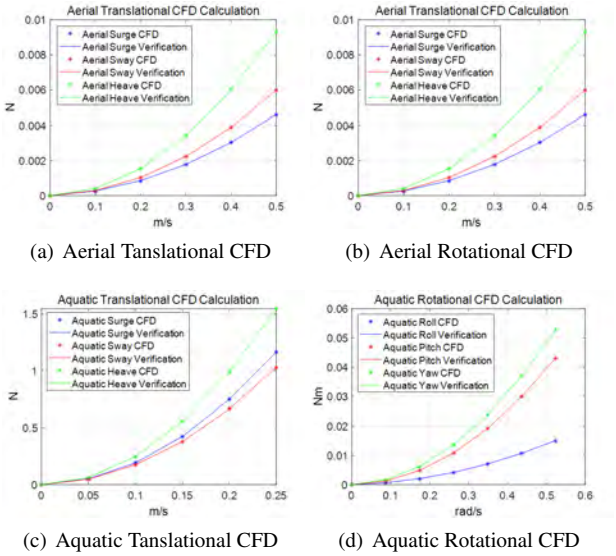

(a) Aerial Tanslational CFD (b) Aerial Rotational CFD

(c) Aquatic Tanslational CFD (d) Aquatic Rotational CFD

Fig. 8: Fitting of calculation results.

is calculated. Since the motion state of 100 % heave mode is relatively simple, calculation of this status is not mentioned in this paper. Due to the layout of TJ-FlyingFish, velocity v is difficult to generate in surge mode. Similarly, in sway mode, the proportion of velocity u is also small. Types of motion that can be generated by the surge and sway modes are very similar. Therefore, in subsequent parts, we calculate operating points for surge mode motion. For the motion of the operating point, as is widely accepted, velocity derivatives in the body-fixed system is 0. Under such constraints, possible motion can be divided into two categories. The first is uniform linear motion, which is also represents for trimming points. The other is stable curved motion with unchanged velocities in body-fixed coordinate. Details of calculation are shown in following parts.

6.1 Calculation of Operating Points

The calculation of operation points is carried out on MATLAB software. For all operation points, velocities in 6-DoF remain constant. Therefore, this calculation is transformed into a problem of solving equations with a series of variables. Converted from steady-state dynamics model, equations are organized as:

$$X_P = X_D - m[vr - wq - g(1 - \frac{\rho V}{m})\sin\theta] \tag{51}$$

$$Y_P = Y_D - m[wp - ur + g(1 - \frac{\rho V}{m})\cos\theta\sin\phi] \tag{52}$$

$$Z_P = Z_D - m[uq - pv + g(1 - \frac{\rho V}{m})\cos\theta\cos\phi] \tag{53}$$

$$K_P = K_D - \rho g V z_B \cos\theta\sin\phi; \tag{54}$$

$$M_P = M_D - \rho g V z_B \sin\theta; \tag{55}$$

$$N_P = N_D; \tag{56}$$

The left side of equations are force and moment generated by propulsion system. According to equations (35) to (40), this part can be converted into a combination of motor speeds and tilting angles. In this way, six equations are established.

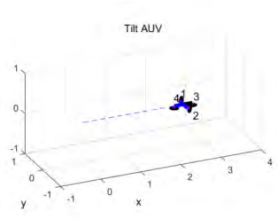

(a) Motion 1 trajectory

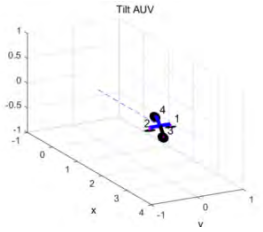

(b) Motion 3 trajectory

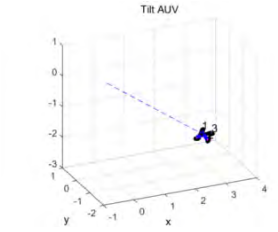

(c) Motion 8 trajectory

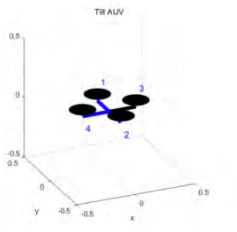

(d) Simplified vehicle shape

Fig. 9: Trimming results of uniform linear motion

In our calculation, we set the speed of the 6-DoF as certain value, and set the motor speed and tilt angles related to the propulsion system as 8 variables. Ignore the effect of ambiguity, we use Matlab to solve the equations and calculate possible operating points. The rationality of these operating points is checked with kinematics and dynamics models and visualization module built in Simulink. Calculation results are presented in following parts.

6.2 Calculation Results of Trimming Points

For surge mode motion, the simplest trimming points are motion along the horizontal direction of the ground coordinate system, which is corresponding to motion 1 in Table 1. In addition, as shwon in motion 2 and 3 in Table 1, in horizontal motion, the vehicle can also generate a pitch or roll angle. Due to the presence of β_3 and β_4, the resulting moment balances the moment caused by the attitude change. The trajectory in simulation and tilting status of motion 1 and 3 are shown in figure 9 (a) and (b).

Apart from the horizontal motion, the vehicle is able to perform oblique motion in ground coordinate system. Movement in the vertical direction is included. Calculation results of operating points are shown in motion 4 to 8 in Table 1. The corresponding simulation result is shown in Figure 9 (c). From these trimming points, the possibility of the vehicle performing uniform linear motion in aquatic 3D space is verified.

6.3 Calculation Results of Operating Points

In addition to the trimming points of uniform linear motion, TJ-FlyingFish can also generate stable curved motion, which is the operating points proposed in this part. These motion include circular and spiral motion. Through the cooperation of the four AAPUs of the propulsion system, a stable moment in yaw is generated on the rigid body of the vehicle, so theoretically this stable circular motion will be generated. On this basis, if the vehicle has a certain w in body-fixed system, it will produce a stable spiral motion. Motion 9 in Table 1 is a circular motion, which is shown in Figure 10 (a). The spiral motion is shown in motion 10, corresponding simulation is shown in Figure 10 (b).

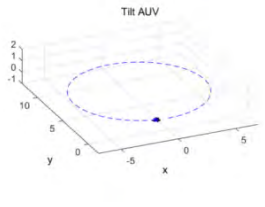

(a) Motion 9 trajectory

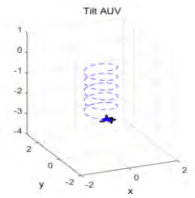

(b) Motion 10 trajectory

Fig. 10: Calculation results of curve motion

6.4 Analysis of Calculation Results

In the above sections, we presented stable motion trajectories that TJ-Flyingfish can generate. The trimming points included in the table 1 are only a small part of steady motion and there are more uniform linear motion that can be achieved in actual works. The existence of multiple steady linear motion means that TJ-FlyingFish is easy to reach a steady state, which means superior controllability of the vehicle. In addition, the vehicle is able to theoretically generate stable circular and spiral motion, which is a verification for the high maneuverability of the aircraft. These calculation results show great potential of TJ-FlyingFish, which can serve as a theoretical basis for control design.

7 Conclusion

We have presented in this paper a modeling method combining first-principle modeling, experiment and CFD for cross-medium vehicles. By deriving the first-principle model of the vehicle, model structure and unknown parameters are determined. For parameter estimation, experimental methods are used to identify the hardware-related parameters, CFD methods are applied to calculate hydrodynamic parameters. These methods together build a mathematical model for analysis. For TJ-FlyingFish designed by our group, a comprehensive dynamics model is established for aerial and aquatic motion. Base on these modeling results, some of the operating points for aquatic motion are explored, typical motion and corresponding operating points are proposed. Our future research is to establish a more accurate and comprehensive dynamics model of cross-medium vehicles and to design sophisticated control systems for advanced missions.

References

[1] Y. H. Tan and B. M. Chen, "Survey on the development of aerial-aquatic hybrid vehicles," *Unmanned Systems*, Vol. 9, pp. 263-–282, 2021.

[2] H. Alzu'bi, I. Mansour and O. Rawashdeh, "Loon copter: Implementation of a hybrid unmanned aquatic-aerial quadcopter with active buoyancy control," *Journal of Field Robotics*, Vol. 35, pp. 764–778, 2018.

[3] Y. H. Tan and B. M. Chen, "A morphable aerial-aquatic quadrotor with coupled symmetric thrust vectoring," *Proceedings of the 2020 IEEE International Conference on Robotics and Automation (ICRA)*, Paris, France, pp. 2223–2229, 2020.

[4] Y. H. Tan and B. M. Chen, "Thruster allocation and mapping of aerial and aquatic modes for a morphable multi-

Table 1: Operating Point List

motion	u	w	r	ϕ	θ	β_1	β_2	β_3	β_4	ω_1	ω_2	ω_3	ω_4
1	0.5	0	0	0	0	79.72	-75.30	0	0	2056.42	2100.45	623.62	250.03
2	0.5	0	0	5	0	77.58	-76.52	-14.55	10.55	2093.99	2065.68	615.83	226.39
3	0.5	0	0	0	45	56.79	-53.77	2.22	1.12	844.98	840.82	1257.60	2054.42
4	0.5	0	0	0	5	80.62	-76.18	0	0	2009.88	2047.86	589.36	418.32
5	0.5	0.5	0	0	0	72.96	-66.94	0	0	2172.57	2094.28	2569.76	2405.14
6	0.5	0.5	0	0	0	51.12	-49.34	1.21	1.41	2381.47	2498.36	1956.01	1757.16
7	0.5	0	0	15	10	72.89	-80.05	-43.75	32.18	2028.53	1963.22	492.73	458.33
8	0.5	0.5	0	15	10	44.90	-47.45	-9.04	4.36	2508.27	2367.82	1733.74	1741.82
9	0.5	0	5	0	0	86.22	-81.71	-2.12	9.10	2038.04	2066.91	892.65	585.08
10	0.5	0.06	20	0	0	82.24	-78.39	-11.13	38.46	2042.25	2086.86	799.64	567.66

modal quadrotor," *IEEE/ASME Transactions on Mechatronics*, Vol. 25, pp. 2065–2074, 2020.

[5] X. Liu, M. Dou, D. Huang, B. Wang, J. Cui, Q. Ren, L. Dou, Z. Gao, J. Chen and B. M. Chen, "TJ-FlyingFish: Design and implementation of an aerial-aquatic quadrotor with tiltable propulsion units," To be Presented at *the 2023 IEEE International Conference on Robotics and Automation (ICRA)*, London, UK, 2023.

[6] R.-A. Peloquin, D. Thibault and A. L. Desbiens, "Design of a passive vertical takeoff and landing aquatic UAV," *IEEE Robotics and Automation Letters*, Vol. 2, pp. 381–388, 2017.

[7] D. Parry, *Navy Launches UAV from Submerged Submarine*, US Naval Research Laboratory News Release, 2013.

[8] D. Lu, C. Xiong, H. Zhou, C. Lyu, R. Hu, C. Yu, Z. Zeng and L. Lian, "Design, fabrication, and characterization of a multimodal hybrid aerial underwater vehicle," *Ocean Engineering*, Vol. 219, pp. 108324, 2021.

[9] M. Guo, Y. Su and D. Gu, "System identification of the quadrotor with inner loop stabilisation system," *International Journal of Modelling, Identification and Control*, Vol. 28, pp. 245–255, 2017.

[10] T. I. Fossen, *Handbook of Marine Craft Hydrodynamics and Motion Control*, John Wiley & Sons, 2011.

[11] M. Nomoto and M. Hattori, "A deep ROV 'DOLPHIN 3K': Design and performance analysis," *IEEE Journal of Oceanic Engineering*, Vol. 11, pp. 373–391, 1986.

[12] K. Rhee, H. K. Yoon, T. Sung, S. H. Kim, and J. N. Kang, "An experimental study on hydrodynamic coefficients of submerged body using planar motion mechanism and coning motion device," *Proceedings of the International Workshop on Ship Manoeuvrability at the Hamburg Ship Model Basin*, pp. 1–20, 2000.

[13] J. P. Avila, D. C. Donha and J. C. Adamowski, "Experimental model identification of open-frame underwater vehicles," *Ocean Engineering*, Vol. 60, pp. 81–94, 2013.

[14] R. Yang, B. Clement, A. Mansour, H. Li, M. Li and N. Wu, "Modeling of a complex-shaped underwater vehicle," *Proceedings of the 2014 IEEE International Conference on Autonomous Robot Systems and Competitions*, Espinho, Portugal, pp. 36–41, 2014.

[15] E. Y. Hong, T. K. Meng and M. Chitre, "Online system identification of the dynamics of an autonomous underwater vehicle," *Proceedings of the 2013 IEEE International Underwater Technology Symposium*, Tokyo, Japan, pp. 1–10, 2013.

[16] K. Shibuya, Y. Kado, S. Honda, T. Iwamoto and K. Tsutsumi, "Underwater robot with a buoyancy control system based on the spermaceti oil hypothesis," *Proceedings of the 2006 IEEE/RSJ International Conference on Intelligent Robots and Systems*, Beijing, China, pp. 3012–3017, 2006.

[17] Y. Singh, S. K. Bhattacharyya, and V. G. Idichandy, "CFD approach to modelling, hydrodynamic analysis and motion characteristics of a laboratory underwater glider with experimental results," *Journal of Ocean Engineering and Science*, Vol. 2, pp. 90–119, 2017.